Proceedings of
ASME TURBO EXPO 2002
June 3-6, 2002, Amsterdam, The Netherlands

2002-GT-XXX

EFFECTS OF FLOW INJECTION FROM OUTER CASING UPON TURBINE NOZZLE VANE FLOW FIELD

K. Funazaki and C.F.F. Favaretto
Department of Mechanical Engineering
Iwate University
Morioka, Japan

T. Tanuma
Steam Turbine Design
Toshiba Corporation
Yokohama, Japan

ABSTRACT

In the present paper steady three-dimensional numerical calculations were performed in order to investigate the effects of flow injection from the outer casing upon turbine nozzle vane flow field. Several test cases were analyzed by applying different nozzle vane configurations such as the blade lean, injection slot width and distance from the leading edge. Numerical simulations were conducted considering the no injection case, 5% and 10% main stream flow injection from the outer casing. The impact of the flow injection design variables and the blade lean angle on the aerodynamic loss in terms of the energy loss coefficient and the outlet flow angle were analyzed through a parametric study.

NOMENCLATURE

Abbreviations

ACM	additive correction multigrid
AMG	algebraic multigrid
HP	high pressure (stage)
inj	(flow) injection
IP	intermediate pressure (stage)
LE	leading edge
neg	negatively
PAC	physical advection correction
PS	pressure side
pos	positively
SS	suction side
SSG	Speziale, Sarkar, Gatsi
UDS	upwind differencing scheme

Symbols

c	[m]	chord
f		function of q
L_ε	[m]	eddy length scale
P	[Pa]	pressure
q	%	injection flow rate
Re		Reynolds number ($= u_2 c_x / \nu$)
s	[m]	slot width
Tu		turbulence intensity
u	[m/s]	absolute velocity
α	[^{0}]	flow angle
β	[^{0}]	blade lean angle
Δ		deviation
γ		specific heat ratio
ν	[m^2/s]	kinematic viscosity
ξ		energy loss coefficient

Subscripts

0	stagnation condition
1, 2	inlet, outlet
x	axial

Superscripts

–	total average

INTRODUCTION

In some combined cycle steam turbines, injection flows (from 5 to 15% of main mass flow rate) from steam generators are induced between turbine stages.

The upstream steam injected from the outer casing is usually at a different temperature and velocity than the main flow. Since the injected steam and the main flow are not completely mixed in the vicinity of the nozzle vane leading edge, pitchwise and spanwise variations of the mass flow and the unsteadiness of the inlet flow angle occur (Fig.1). Such

variation will change the turbine stage operating conditions, affecting the blading flow pattern and efficiency.

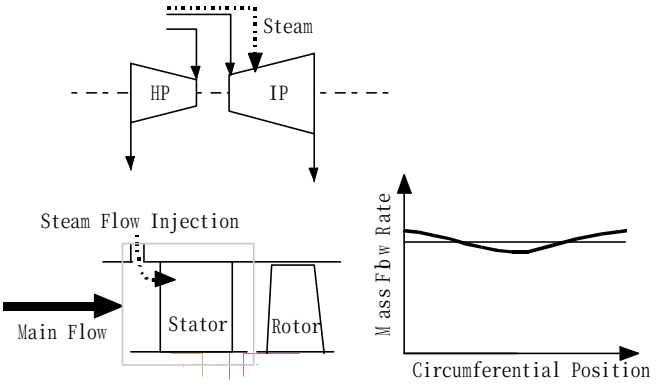

Figure 1: Flow Injection Schematic Diagram.

Due to the lack of information on the flow field generated by the flow distortion and the increasing demand of the steam turbine companies in designing high performance machines, a remarkable number of authors have been investigating the inlet and outlet flow distortion phenomena by applying numerical simulation or performing experimental analysis.

In the work of Hirai et al. [1], numerical simulation was used to investigate the effect of circumferential positions of inlet hot streaks to a single stage turbine. The pressure loss due to unsteady flow for a transonic rotor with inlet total pressure distortion was also analyzed. Adamczyk [2] outlined the unsteady aerodynamic interaction effects on turbomachinery blade life and performance.

Moser [3] investigated distorted flow conditions caused by asymmetric exhaust and by ribs in the radial and circumferential direction by using pneumatic probes. Zeschky and Gallus [4] determined the effects of the outlet distortion provided from the stator exit on the turbine rotor by using three-dimensional hot-wire and pneumatic probes. The formation of the passage vortices in the rotor were found to be strongly influenced by the non-uniform stator outlet flow which caused the accumulation of low-energy fluid in the rotor wake close to midspan.

Biesinger & Gregory-Smith [5] analyzed the effect of upstream tangential blowing in a turbine cascade of rotor blades. According to their experiments, blowing at low velocity serves to increase the amount of low energy fluid, resulting in a rise in secondary flow and loss. As the blowing rate was increased, the positive streamwise vorticity started to counteract with the secondary vortex, and a reduction in secondary kinetic energy and loss was achieved. The injection angle was also analyzed by the authors, the low angle being more effective than the high angle, keeping the blowing jet closer to the end wall at inlet to the cascade.

In order to minimize the loss effects caused by the flow distortion several design techniques have been developed. For instance, Harvey et al. [6] proposed a linear design system which generates end wall non-axisymmetric profiles in order to reduce secondary flows, in particular secondary kinetic energy and exit angle deviations. The final profiled hub wall design presented in the paper showed a reduction of the size of the passage vortex, decreasing the loss for almost one quarter of the blade span.

Other design techniques which can be comparable to the non-axisymmetric profile are blade leaning, skewing and bowing (compound lean). Harrison [7] presented a study on the actual contribution of the blade lean on the reduction of the loss coefficient. It was found that simple lean reduces velocities and loss generation substantially at one end wall and increases them at the opposite wall. Compound lean reduced the enwall and downstream mixing losses, increased the flow turning and substantially reduced spanwise variations on the span angle.

Songtao et al. [8] performed a similar study considering two bow angles. It was shown that although blades with positively bow angle can decrease the end wall loss, the midspan loss will increase.

The referenced papers are very informative but unfortunately they do not present an investigation of the effects of the flow injection on the flow field around leaned nozzle vanes. Flow injection from the outer casing upstream leaned nozzle vanes can be an effective technique to minimize the drawback of the inlet distortion. In the present study, the influence of the flow injection design variables such as slot width and distance from the leading edge as well as the blade lean on the aerodynamic loss and the outlet flow angle were analyzed.

METHODOLOGY

Numerical simulations were conducted on several turbine nozzle vane configurations. The following design parameters were analyzed: blade lean (Fig.2), injection slot width and distance from the leading edge.

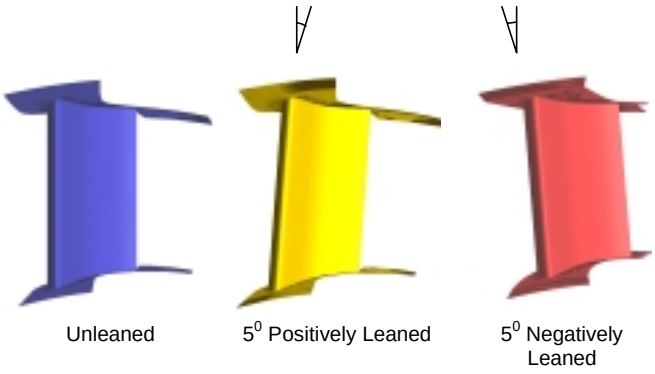

Figure 2: Unleaned and leaned nozzle vanes.

Initially, no flow injection was considered and the results for the unleaned nozzle vane were compared to the experimental data. Once the boundary conditions and the flow quantities were validated, calculations were performed for 5%

and 10% main stream injected flow combining the different design parameter values.
The influence of the design parameters on the aerodynamic performance of turbine nozzle vanes was then analyzed. The outlet flow angle distortion (the difference between the outlet angle for the analyzed case and the no injection case) was also evaluated.

NUMERICAL SIMULATION

Grid Generation

A structured multi-block grid system was generated with the *CFX-TurboGrid 1.0* software. For all analyzed cases the computational domain consisted of an H-type grid block extending from the inlet to downstream of the injection slot (16x11x50 *INBLOCK*), an O-type grid block surrounding the blade (256x17x50 *MAIN*), a C-type grid block around the O-type grid from downstream the slot to the trailing edge (201x16x50 *CGRID*) and two H-type grid blocks (71x31x50 *TEDPS* and 31x31x50 *TEDSS*) extending from the trailing edge to the outlet region on the pressure and suction sides (Fig.3a).

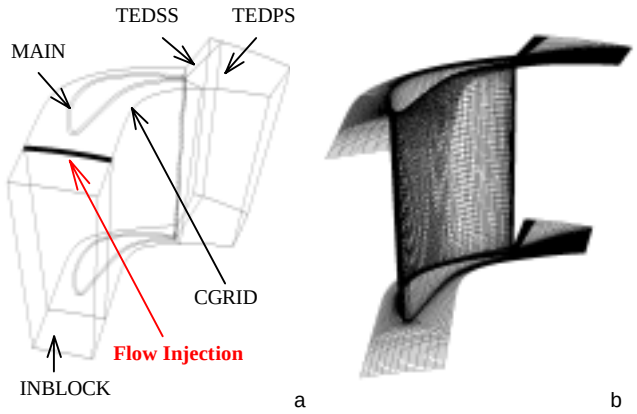

Figure 3: Grid block configuration and grid system.

Number of grid points	Streamwise direction	Pitchwise direction	Spanwise direction
21	1.54 %	1.23 %	---
30	---	---	1.19 %
36	1.19 %	---	---
50	---	---	1.19 %
61	0.85 %	1.19 %	---
70	---	---	1.19 %
81	0.78 %	1.19 %	---

Table 1: Percentage difference between the numerical results and the experiments (total pressure downstream the nozzle at midspan).

In spite of using a logarithm wall function, the mesh seeding was performed so that the y^+ of the first near wall node was approximately 30. Grid independency analysis was performed by changing the grid density in the streamwise, pitchwise and spanwise directions. Table 1 shows the percentage difference between the total pressure downstream the nozzle at midspan from the calculations and the experiments. In Fig.3b, for the sake of clarity, the final grid system is shown only on the blade, hub and tip surfaces.

Computational Code

The three-dimensional, steady-state, Reynolds-averaged, compressible Navier-Stokes equations were solved with the *CFX-TASCflow 2.10.0* computational code. Several numerical analyses of the flow field inside turbomachinery were performed by using this code, as described by Labrecque et al. [9], Casciaro et al. [10], von Hoyningen–Huene and Hermeler [11], Casciaro et al. [12] and Favaretto [13].

Concerning the domain discretization, the code uses a finite volume method based on the finite elements method in order to enable a more accurate modeling of the geometry. The diffusive terms are calculated by the conventional finite elements method using shape functions to calculate the derivatives. In the same fashion, the pressure gradient terms in the momentum equations are also determined.

For the advective terms, the *UDS* (Upwind Differencing Scheme) with the *PAC* (Physical Advection Correction [14]) scheme was employed. This discretization method produced the most accurate solution among the other methods available in the code.

The solution algorithm uses the *AMG* (Algebraic Multigrid [15]) method, which is based on the *ACM* (Additive Correction Method [16]) correction strategy. The algorithm is fully coupled, ie., the momentum and continuity equations are solved simultaneously. The unstructured data structure allows connectivities in periodicity and grid interface regions to be solved in a fully implicit fashion. Detailed information on the theoretical basis of the software can be found in the CFX-TASCflow Theory Documentation [14].

Boundary Conditions

The boundary conditions employed were based on the experimental data. For the inlet region, total pressure, total temperature, flow angle, inlet turbulence intensity (*Tu*) and inlet eddy length scale (L_ε) were prescribed. The values for the inlet turbulence intensity and inlet eddy length scale were investigated by performing several simulations combining difference values. A similar study was performed Casciaro et al. [10] using the same software. In the present study it was found that Tu=5% and L_ε=0.05m presented the best agreement with the experimental data. For the outlet region, static pressure was prescribed.

Concerning the flow injection cases, the velocity was prescribed normal to the outer casing and its magnitude was calculated as 5% and 10% of the main stream flow rate (Fig.3a). The same value for the total temperature at the inlet was prescribed in the flow injection region. The average Reynolds number for all cases was 430,000.

The blade, hub and tip wall regions were assumed as adiabatic and the non-slip condition was applied. A logarithm wall function was used for the near-wall grid points. For the pitchwise boundaries, periodic boundary condition was applied.

Turbulence Model

Due to the highly turbulent region behind the trailing edge, where the flow must be regarded as non-isotropic, the Reynolds stress second-order closure turbulence model was employed. In addition to the anisotropic turbulence calculation feature, the model can solve the production term without any modeling. In the reference Amano et al. [17] a comparison between this particular turbulence model and the κ-ε model applied to a steam turbine flow field calculation is presented, the former being more suitable for the problem.

In a similar fashion as performed by Hildebrandt and Fottner [18], a study on the turbulence model was also performed. Computations were performed by employing the κ-ω model with the shear stress transport model and the Kato-Launder production model [19], and the Reynolds stress model using the *SSG* (Speziale, Sarkar and Gatsi [20]) quadratic model with scalable log-law wall function. Among all tested models, the Reynolds stress *SSG* model with scalable log-law wall function produced the best agreement with the experiments and was adopted as the standard model for all analysis cases.

RESULTS

Validation with Experimental Data

The numerical results for the unleaned nozzle vane with no flow injection from the outer casing were validated with the experimental data measured at the Heavy Apparatus Engineering Laboratory of Toshiba Corporation.

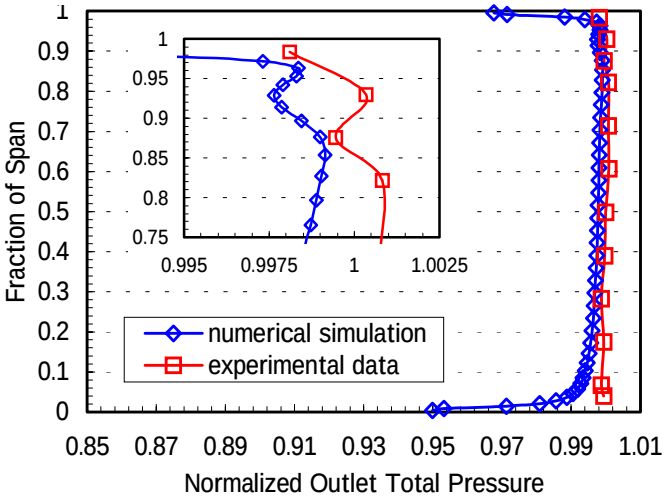

Figure 4: Normalized outlet total pressure distribution.

Inlet total pressure, outlet static pressure, outlet total pressure and outlet absolute velocity measurements were performed using the experimental apparatus described in the work of Tanuma et al. [21]. The difference between the numerical simulation and the experiments for the normalized outlet total pressure at midspan was less than 0.2 % (Fig.4). The normalized results described throughout the text were divided by the respective values at midspan for the unleaned blade with no flow injection case.

Flow Injection

The effect of flow injection upstream the nozzle vanes of a turbine stage can be regarded as a technique to reduce the profile loss, as described by Biesinger & Gregory-Smith [5]. According to the authors, the effect of the increasing blowing is first to thicken the inlet boundary layer, giving greater secondary flow and more loss, and then as a re-energisation of the inlet boundary layer takes place together with increasing counter streamwise vorticity, the passage vortex is progressively weakened, with a corresponding reduction in loss. However, flow injection may also cause additional loss depending on the injection flow rate, the injection angle and the geometry of the downstream edge of the injection slot.

In the present paper, computations were performed for the no injection case, 5% and 10% main stream injection flow. In order to have a better understanding of the flow injection effects, numerical simulations were carried out for the straight blade first.

Fig.5 presents the streakline plots for the no injection and the 10% flow injection cases. The streaklines were emitted from the most upstream nodes in the vicinity of the end wall.

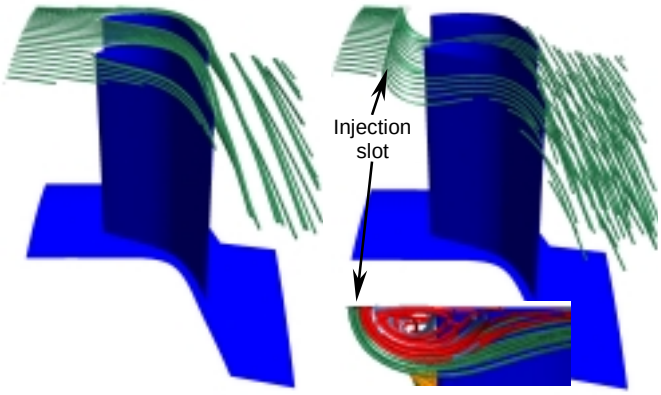

Figure 5: Streaklines for the no injection and 10% flow injection cases.

In Fig. 5a one can observe the trajectory of the passage vortex due to the cross-pressure gradient. In Fig.5b, due to the flow injection, the same clear structure cannot be observed. The fluid particles departing from far upstream deviate their trajectory near the upstream of the injection slot. In the bottom part of Fig. 5b a projected view of the streakline plot on the pitchwise plane is presented. These streaklines were emitted from the injection slot and different colors were used for each

one quarter of the slot area. It can be evidenced that approximately one half of the streaklines (green) follows the same behavior as the streaklines emitted from the far upstream and the other half (red) recirculates. As a consequence, the outlet flow angle for the injection case changed significantly. From Fig.5b, it seems that some streaklines close to the suction side of the nozzle vane remained with their initial orientation, keeping the outlet flow angle unchanged. At different pitchwise locations, however, the streaklines are gradually deviated.

Fig.6 shows the normalized pitchwisely mass-averaged outlet flow angle for the straight blade. The curves indicate the penetration of the injection flow, which is characterized by the increase of the magnitude of the outlet flow angle from 70% span to the tip and the displacement of the maximum point outward from the wall. The gradual change in turning from the no injection to the 10% injection case is a consequence of the recirculation region downstream the injection slot, which actually acts as a wall. The streaklines emitted from the far upstream, when encountering such region, are compressed from hub to the periphery of the vortices. As the main stream fluid passes through the streamwise plane crossing the vortex core, it is decelerated due to the adverse pressure gradient, analogous to a divergent channel. The outlet axial velocity profiles (not shown in this paper) indicate a relative deceleration of the flow field for the 10% injection case from the casing to approximately 85% span with a compensatory acceleration from 85% to 60% span.

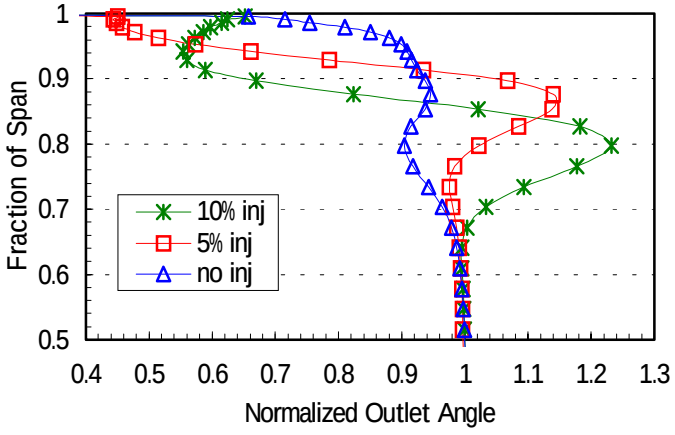

Figure 6: Normalized pitchwisely mass-averaged outlet flow angle for the straight blade.

Blade Lean

The use of leaned blades has a significant effect upon blade loading and on the loss generation, as reported by Harrison [7]. Furthermore, Songtao et al. [8] described the influence of the bow angle on the stability of the passage vortex, which plays an important role on the overall loss. It was shown that the passage vortex for the positively bowed blade cascade was more compact than in a straight blade, which diminished the range and mass exchanged between the passage vortex and high-energy fluid around it. Such effect decreased the loss generated by the mixture of the high-energy fluid and the low-energy fluid in the passage vortex, thus reducing the secondary loss. Considering the findings of the cited authors, the blade lean is expected to provide a significant loss reduction depending on the lean direction, specially for the injected flow conditions where additional secondary losses are generated. As a counterpart of the expected gain in aerodynamic performance, the lean angle may cause an outlet flow angle deviation ($\Delta\alpha_2$), which is the difference between the outlet flow angle of the leaned and the unleaned blade. The evaluation of $\Delta\alpha_2$ is an important information for the turbine designer since a high flow angle deviation at the nozzle outlet will cause the rotor to operate at off-design conditions, reducing substantially the stage efficiency.

In order to quantify the effects of the lean angle on the energy loss and the outlet flow angle deviation, computations were performed for the no injection case, 5% and 10% main stream injection flow.

Fig.7 shows the normalized pitchwisely mass-averaged outlet flow angle for the unleaned and the two leaned blade configurations for the 10% flow injection case. It can be noted that an inflection point at midspan distinguishes the behavior due to the lean angle. The positively leaned blade presented a higher outlet flow angle near the hub whereas the opposite behavior was found for the negatively leaned case. The same conclusions were drawn for the no flow injection and the 5% flow injection cases.

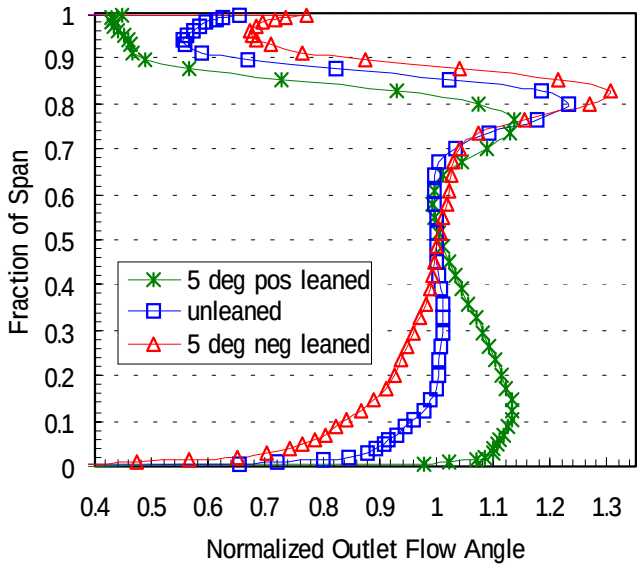

Figure 7: Normalized pitchwisely mass-averaged outlet flow angle for the 10% flow injection case.

Minimizing the outlet angle deviation is a crucial task when analyzing the advantage of the blade lean design technique. After evaluating the spanwise average of the curves in Fig.7 and the curves for the no injection and 5% flow injection cases it

was found that leaning the blade in the negative direction produces a lower $\Delta\alpha_2$ than leaning in the positive direction (Fig.8). For instance, considering the 10% flow injection case, the outlet flow angle deviation was almost zero as the blade was leaned to the negative side whereas this difference was approximately 3% higher for the positively leaned. Fig.8 also shows that the 5% and 10% injection curves are closer to each other than the no injection and the 5% injection case. These results suggest that increasing the injection flow rate will increase the outlet flow angle up to a certain limit from which $\Delta\alpha_2$ can be regarded as independent on the injected flow rate. The investigation of such limit has not been performed in the present study.

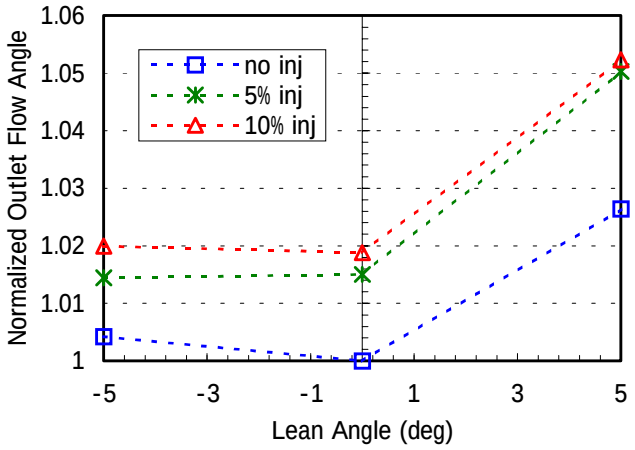

Figure 8: Normalized outlet flow angle for the leaned nozzle vanes.

The determination of the energy loss coefficient (Eq.1) was based on model adopted by Tanuma et al. in the study of gas turbine cascades with coolant ejection [21] and on the model described in the JSME Data Book [22].

$$\xi = \frac{\left(P_{01}/P_{02}\right)^{\frac{\gamma-1}{\gamma}} - 1}{\left(P_{01}/P_{2}\right)^{\frac{\gamma-1}{\gamma}} - 1} \qquad (1)$$

where: ξ is the energy loss coefficient, P_{01} the inlet total pressure, P_{02} the outlet total pressure, P_2 the outlet static pressure and γ the specific heat ratio.

Fig.9 presents the normalized pitchwisely mass-averaged energy loss coefficient. The inlet values for the coefficient evaluation were taken at a plane in the vicinity of the slot downstream edge. It can be noted that the energy loss coefficient curves, in a similar fashion as for the outlet flow angle, can be distinguished by two zones. From approximately midpan to the hub the positively leaned blade presented a lower energy loss coefficient whereas from midspan to tip the aerodynamic performance was substantially improved by the negatively leaned blade.

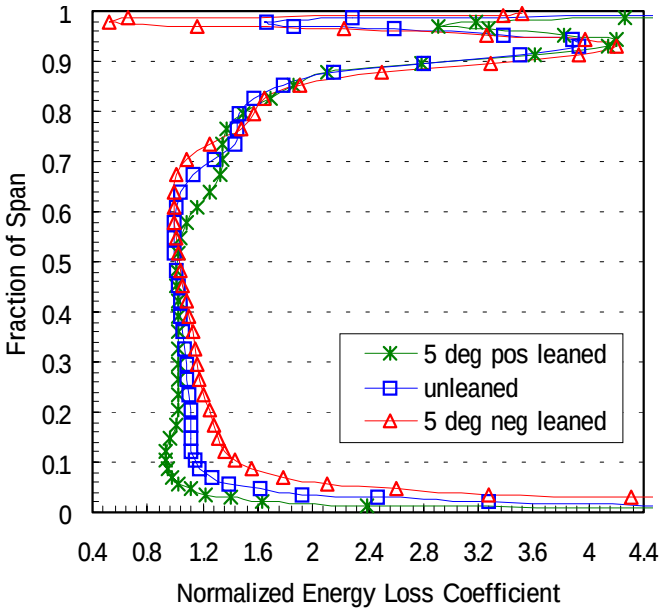

Figure 9: Normalized pitchwisely mass-averaged energy loss coefficient for the 10% flow injection case.

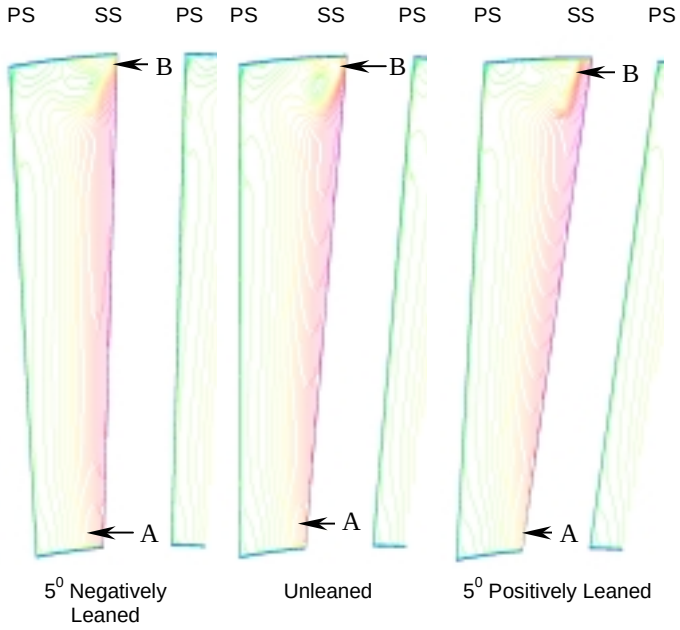

Figure 10: Absolute velocity contours for the 10% flow injection case at 50% axial chord.

In Fig.10 one can observe the absolute velocity contours for the three nozzle configurations with 10% flow injection for a plane at 50% of the axial chord. The contours show a higher velocity gradient for the negatively leaned blade near the hub, which gradually decreases as the blade is leaned in the positive direction (contour A). An opposite behavior was found at the tip, where the highest gradient occurs for the positively leaned

blade (contour B). The static pressure distribution (not shown in this paper) presented an analogous behavior, which indicates that the cross-pressure gradient can be reduced in the near wall regions depending on the blade lean direction. Reducing the cross-pressure gradient will weaken the passage vortex and thus reduce secondary losses near the end walls. Such phenomena was previously evidenced by the energy loss coefficient curves (Fig.9).

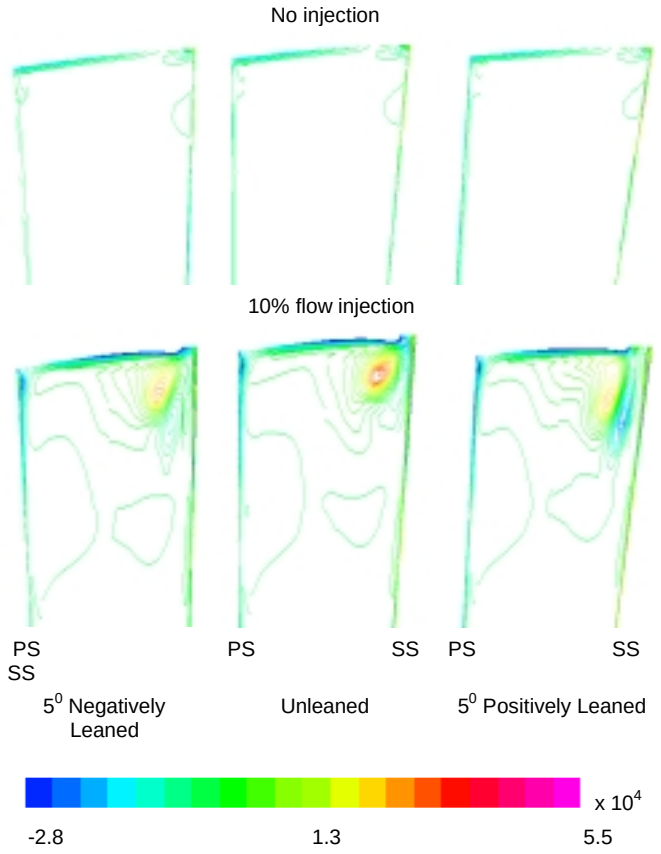

Figure 11: Streamwise vorticity contours for no injection and 10% flow injection cases at 50% axial chord (from 70% span to tip).

The mass flow near the tip for the positively leaned blade (leaned to the pressure side) was increased, which will affect the structure of the additional vortex generated due to the flow injection. In Fig.11 one can observe the axial vorticity contours for the no injection and 10% injection cases at 50% axial chord. Concerning the no injection case, a small change in the passage vortex structure can be observed. The vortex size for the positively leaned blade was slightly reduced comparing to the unleaned and negatively leaned cases. For the 10% flow injection case such characteristic is more clearly observed. In spite of the increased mass flow rate at the tip for the positively leaned blade, the size of the vortex due to the flow injection was substantially reduced. The vortical structure is pushed away from the suction surface and the positive and negative vorticity contours (red and blue lines, respectively) are confined in a smaller region.

Initially, in order to evaluate the total energy loss coefficient, the curves from Fig.9 and for the no flow and 5% flow injection cases were spanwisely averaged. The use of such approach may arise some contradiction since the inlet values for its evaluation were taken at a plane in the vicinity of the slot downstream edge, where the main flow may not be completely mixed with the injected flow. Taking such fact into account, another model for the total energy loss was proposed (Eq.2). First, the total average of the quantity values at the inlet, at the slot and at the outlet boundaries were evaluated. Next, a weighted average of the total pressure values at the inlet and the slot were performed (Eq.3). The energy loss coefficient was then evaluated by applying the averaged quantities in Eq.2.

$$\bar{\xi} = \frac{\left(\bar{P}'_{01}/\bar{P}_{02}\right)^{\frac{\gamma-1}{\gamma}} - 1}{\left(\bar{P}'_{01}/\bar{P}_{2}\right)^{\frac{\gamma-1}{\gamma}} - 1} \qquad (2)$$

$$\bar{P}'_{01} = \frac{\bar{P}_{01}\cdot\bar{\dot{m}}_1 + \bar{P}_{0s}\cdot\bar{\dot{m}}_s}{\bar{\dot{m}}_1 + \bar{\dot{m}}_s} \qquad (3)$$

where: $\bar{\xi}$ is the total energy loss coefficient, $\bar{P}'_{01}$ the weighted averaged inlet total pressure, $\bar{P}_{02}$ the totally averaged outlet total pressure, $\bar{P}_2$ the totally averaged outlet static pressure, $\bar{P}_{01}$ the totally averaged inlet total pressure, $\bar{P}_{0s}$ the totally averaged total pressure at the slot, $\bar{\dot{m}}_1$ the totally averaged inlet mass flow and $\bar{\dot{m}}_s$ the totally averaged mass flow at the slot.

Fig.12 presents the total energy loss coefficient for the leaned nozzle vanes. It can be found that the energy loss coefficient is decreased with increasing lean angle in the positive direction. The slope of the curves in Fig.12 does not seem to be sensitive to the flow injection, ie., the loss is decreased at the same rate. Considering the linear relationship between energy loss and lean angle shown in Fig.12, the following equation below can be deduced:

$$\bar{\xi}(\beta,q) = 0.01\beta + 1 + f(q)$$

$$\text{for } -5^0 \le \beta \le +5^0 \text{ and } 0\% \le q \le 10\% \qquad (4)$$

where: β is the lean angle (°), q is the injection flow rate expressed as a percentage of the main flow and f a function of q.

The dependence of the function f in relation to q has not been investigated yet, which is a motivation for the continuation of the present research.

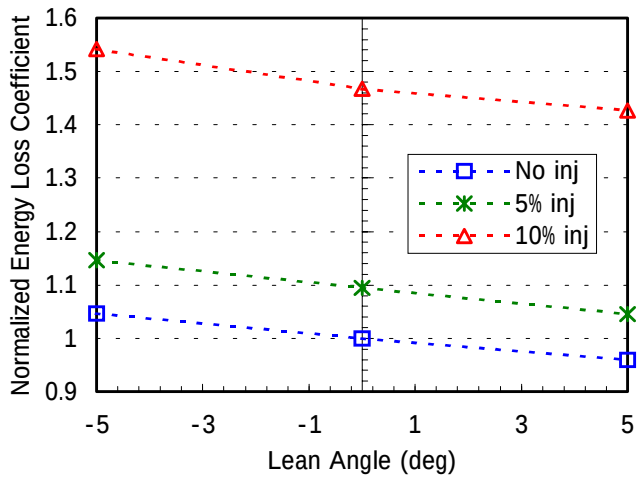

Figure 12: Normalized energy loss coefficient for the leaned nozzle vanes.

Slot Width

The investigation of the slot width was performed for three slot dimensions, the design value *s* (6.25% of the axial chord length), *0.714s* and *0.357s*. The calculations were performed for 5% and 10% flow injection cases.

Fig.13 presents the normalized pitchwisely mass-averaged outlet flow angle for the 10% flow injection case. The relationship among the four curves resemble the results shown in Fig.6. This is rather expected, since increasing the slot width for the same injection flow rate implies in a lower velocity magnitude prescribed at the slot surface.

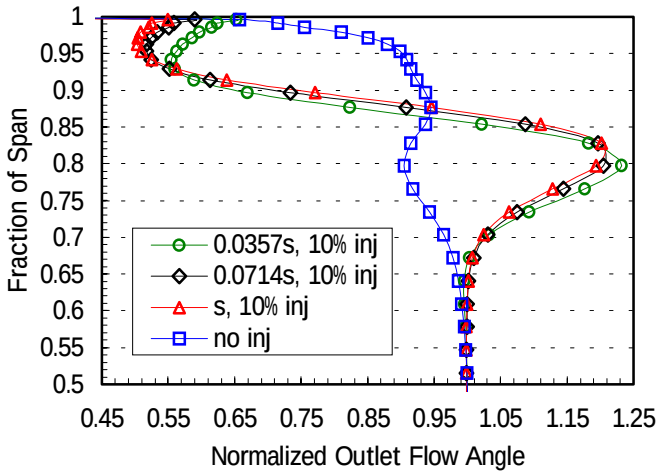

Figure 13: Normalized pitchwisely mass-averaged outlet flow angle for the 10% flow injection case.

In Table 2 the spanwisely averaged normalized outlet flow angle deviation values are presented as a function of the slot width. It can be noted that the relationship between slot width and outlet flow angle changes according to the injection flow rate. Increasing flow injection with increasing slot width has a cost in terms of the outlet flow angle deviation. The results indicate that minimizing $\Delta\alpha_2$ can be accomplished by increasing the slot width and reducing the injected flow rate from at least 5%. It must be noted, however, that the highest outlet flow angle deviation was found to be less than 0.3^0, which may have the same order of magnitude as the blade manufacturing tolerance.

Slot Width	Outlet flow angle deviation (^{0})	
	5% flow injection	10% flow injection
0.375s	0.209	0.261
0.714s	0.19272	0.28742
s	0.184	0.291

Table 2 – Normalized outlet flow angle deviation for the slot width configurations.

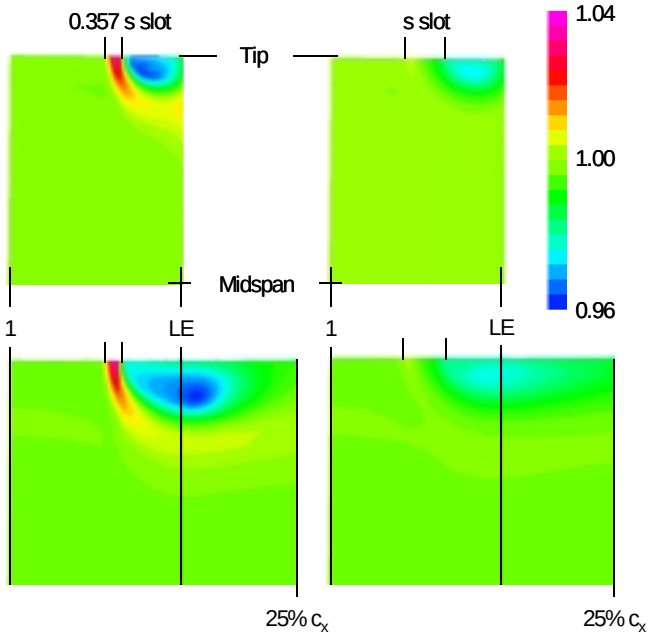

Figure 14: Total pressure distribution upstream the leading edge for the 10% flow injection case (top: 50% pitch, bottom: 0% pitch).

In Fig.14 the total pressure distribution is presented for a plane at two pitch locations[1]. As expected, in spite of the different injection velocity, the averaged total pressure at the outlet of the *0.357s* slot is 2.8% higher than in the *s* slot case. The injected flow from the *0.357s* slot is energizing the main flow thus causing a highly disturbed flow field. Such phenomena results in a low energy fluid region extending from downstream the injection slot to the blade leading edge. In the *s*

[1] In the present text, the 50% pitch location was assumed to be aligned with the leading edge whereas the 0% pitch plane coincides with the periodic boundaries.

slot case, the injected flow partially energizes the main stream from the slot upstream edge to approximately 30% of its extension. From 30% to the slot downstream edge the total pressure is at a slightly lower level than the inlet values and in some regions even lower than the outlet values. The pressure gradient for the *s* slot configuration is not as high as in the *0.357s* case, as a consequence, the flow field becomes more homogeneous.

In Table 3, the spanwisely averaged normalized energy loss coefficient calculated by using Eq.2 is represented as a function of the slot width. It can be noted that increasing the slot width is favorable for reducing the energy loss coefficient.

Slot Width	Normalized Energy Loss Coefficient	
	5% flow injection	10% flow injection
0.375s	1.095	1.467
0.714s	1.047	1.147
s	1.038	1.093

Table 3: Normalized energy loss coefficient for the slot width configurations.

Slot Distance

The influence of the distance between the slot downstream edge and the leading edge on the outlet flow angle deviation and on the energy loss coefficient was analyzed for two configurations, 25% and 50% axial chord (c_x). The calculations were performed for 5% and 10% flow injection cases.

Fig.15 presents the normalized pitchwisely mass-averaged outlet flow angle for the 10% flow injection case. In Table 4, the spanwisely averaged normalized outlet flow angle deviation values are represented as a function of the slot distance. The highest outlet flow angle deviation was found to be less than 0.3^0, thus the same remarks made for the slot width analysis may be considered here. The results roughly show a decrease in $\Delta\alpha_2$ with the increase in the slot distance, as expected.

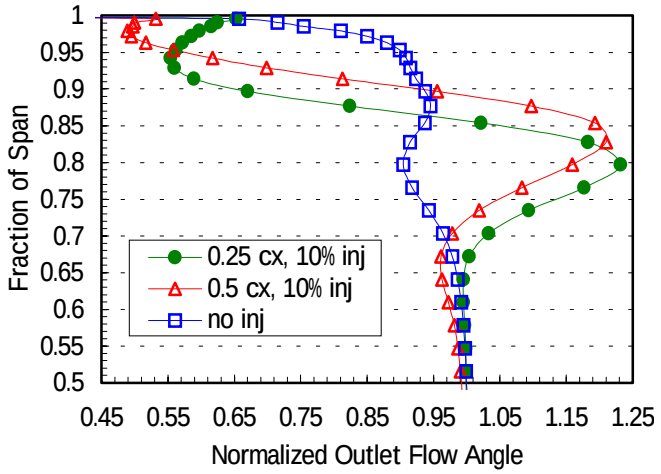

Figure 15: Normalized pitchwisely mass-averaged outlet flow angle for the 10% flow injection case.

Slot	Outlet flow angle deviation (^{0})	
	5% flow injection	10% flow injection
0.25 c_x	0.209	0.261
0.5 c_x	0.195	0.243

Table 4: Normalized outlet flow angle deviation for the slot distance configurations.

Fig.16 shows the normalized total pressure distribution for the $0.25c_x$ and $0.5c_x$ cases. It can be noted that the pressure gradient is lower for the larger slot distance case. In the $0.25c_x$ case the low energy fluid is confined in a smaller region which will generate a higher pressure difference between regions near the slot and the nozzle leading edge.

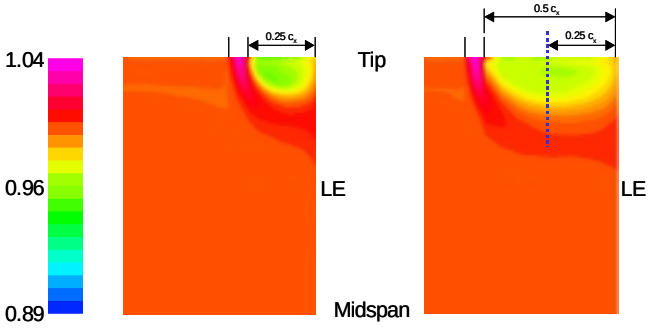

Figure 16: Normalized total pressure distribution upstream the leading edge for the $0.25c_x$ and $0.5c_x$ cases (10% flow injection, 50% pitch).

In Fig.17, the normalized total pressure plots are presented for three streamwise locations, near the leading edge, 50% c_x and near the trailing edge. The figures indicate that a substantial reduction in the total pressure loss for the $0.5c_x$ case is expected for all streamwise locations. For the $0.25c_x$ case, due to the smaller distance from the leading edge the low energy fluid region is expanded in the pitchwise direction causing a higher disturbance in the flow comparing to the $0.5c_x$ case (Fig.17a). At the 50% c_x both cases seemed to present the same core location of the high energy loss region (Fig.17b). In the region near the trailing edge (Fig.17c) the distinct behavior can still be observed. In the $0.5c_x$ case the cross-pressure gradient is increased from pressure side to suction side at almost all spanwise locations. For the $0.25c_x$ case, however, in the low energy region due to the flow injection (from approximately 80% to 90% span) a small valley can be observed in the total pressure distribution (letter *V* in the top left side of Fig.17c).

Fig.17c also shows that the low energy region for the $0.50c_x$ was moved towards the end wall whereas for the $0.25c_x$ case the opposite behavior was observed (letter *L* in the top and right sides of the figure). Such phenomena might be related to the interaction between the passage vortex and the vortex caused by the flow injection.

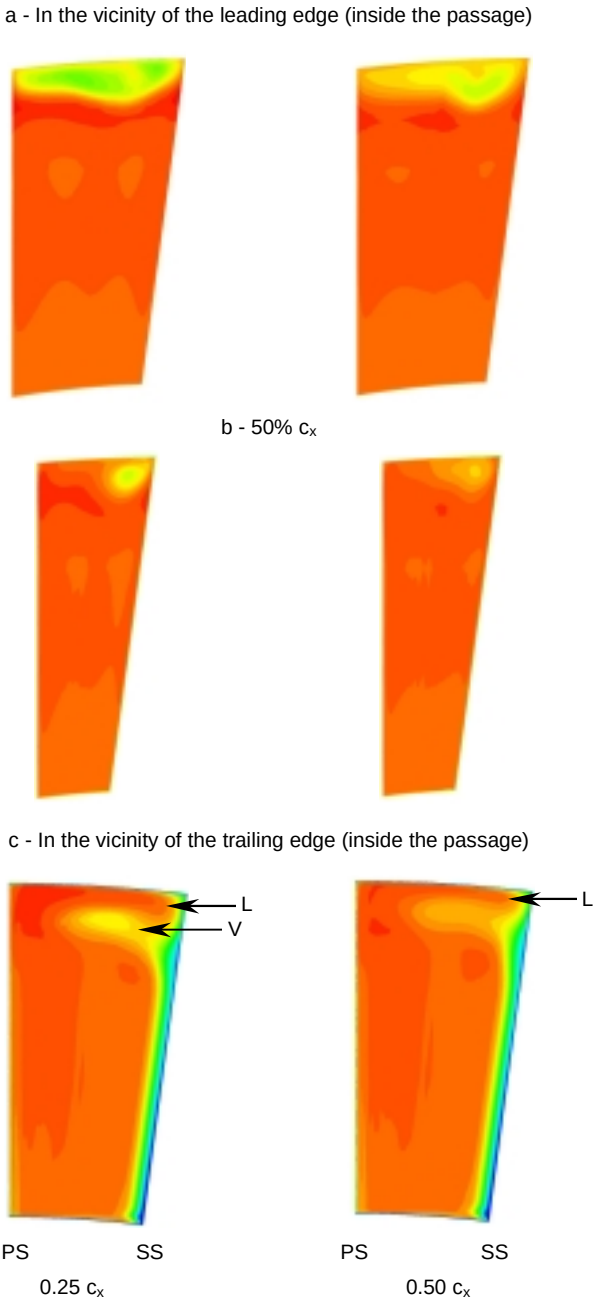

Figure 17: Normalized total pressure distribution for the $0.25c_x$ (*left side*) and $0.5c_x$ (*right side*) cases with 10% flow injection for three streamwise locations.

The larger slot distance from the leading edge attenuates secondary losses by feeding energy to the low energy fluid. This will reduce the pressure gradient and vorticity of the fluid confined between the leading edge and the slot. As a consequence, the pitchwise variation of the total pressure in the vicinity of the leading edge will be reduced, introducing less disturbance to the flow field inside the passage. The total pressure at the outlet will be higher due to the lower profile loss inside the passage and thus the energy loss will be reduced.

The normalized energy loss coefficient values calculated from Eq.2 indicated approximately one percent increase in the loss with increasing slot width for both flow injection cases. The reason for this contradictory result can be explained from Fig.16. Since the slot distance is different for both cases the location where the totally averaged total pressure at the slot $\overline{P}_{0s}$ is also different. For the $0.50c_x$ case the pressure at the slot is higher than for the $0.25c_x$ case, which will result in a higher loss coefficient even though the outlet total pressure is higher. Therefore, a different marker should be used for the slot distance analysis. The development of such model is still a topic to be discussed. In terms of totally averaged outlet total pressure a small gain of less than 0.02 % was obtained for the $0.50c_x$ configuration.

CONCLUDING REMARKS

Extensive numerical simulations were conducted in order to investigate the impact of the injection flow design variables as well as the blade lean on the aerodynamic performance of a turbine nozzle vane.

The blade lean plays a significant role in the reduction of the energy loss coefficient as well as the outlet flow angle deviation. It was found that the negatively leaned blade is more efficient in reducing the profile loss whereas the positively leaned blade produced a smaller outlet flow angle deviation. The injected flow increased the energy loss by shifting the loss curve and maintaining its slope constant.

Concerning the slot width parametric analysis, it was noted that the injection flow rate has a significant influence on the outlet flow angle deviation. For a high flow rate the outlet angle deviation is increased with increasing slot width whereas for lower flow rates the opposite behavior was found. The energy loss coefficient was found to be inversely proportional to the slot width and such characteristic is amplified with increasing injected flow rate.

The slot distance analysis showed that increasing the distance from the leading edge reduces the outlet flow angle deviation and barely increases the totally averaged outlet total pressure.

The present study provided important information for minimizing the energy loss and outlet flow angle deviation due to flow injection upstream the nozzle vanes of a turbine stage. Understanding the impact of flow injection around the nozzle vanes beforehand can not only aid in analyzing the complex flow field in the complete turbine stage, but also reduce computational time considerably.

ACKNOWLEDGMENTS

The second author acknowledges the financial support of the Ministry of Education, Culture, Sports, Science and Technology of Japan (Monbusho).

REFERENCES

[1] Hirai, K., Kodama, H., Nozaki, O., Kikuchi, K., Tamura, A., Matsuo, Y., 1997, "Unsteady Three-Dimensional Analysis of Inlet Distortion in Turbomachinery", AIAA Paper 97-2735.

[2] Adamczyk, J.J., 1992, "Unsteady Aerodynamic Interaction Effects on Turbomachinery Blade Life and Performance", AIAA Paper 92-0149.

[3] Moser, W., 1989, "An Analysis of Outlet Distortion in LP Steam Turbines", ASME Paper 89-GT-237.

[4] Zeschky, J., Gallus, H.E., 1993, "Effects of Stator Wakes and Spanwise Nonuniform Inlet Conditions on the Rotor Flow of an Axial Turbine Stage", ASME Journal of Turbomachinery, Vol. 115, pp. 128-136.

[5] Biesinger, T.E., Gregory-Smith, D.G., 1993, "Reduction in Secondary Flows and Losses in a Turbine Cascade by Upstream Boundary Layer Blowing", ASME Paper 93-GT-114.

[6] Harvey, N.W., 2000, "Nonaxisymmetric Turbine End Wall Design: Part I – Three-Dimensional Linear Design System", ASME Journal of Turbomachinery, Vol. 122, pp. 278-285.

[7] Harrison, S., 1992, "The Influence of Blade Lean on Turbine Losses", ASME Journal of Turbomachinery, Vol. 114, pp. 184-190.

[8] Songtao, W., Zhongqi, W., Guotai, F., 2001, "Numerical Simulation of 3D Flow Field Structure in Turbine Cascade with Bowed Blades", ASME Paper 2001-GT-0442.

[9] Labrecque, Y., Sabourin, M., Deschênes, C., 1996, "Numerical Simulation of a Complete Turbine and Interaction between Components", Modeling, Testing & Monitoring for Hydro Powerplants, Lausanne, Switzerland.

[10] Casciaro, C., Treiber, M., Sell, M., Saxer, A.P., Gyarmarthy, G., 1998, "A Comparison of Experimental with Computational Results in an Annular Turbine Cascade with Emphasis on Losses", ASME Paper 98-GT-146.

[11] von Hoyningen-Huene, M., Hermeler, J., 1999, "Time-Resolved Numerical Analysis of the 2-D Aerodynamics in the First Stage of an Industrial Gas Turbine for Different Vane-Blade Spacings", ASME Paper 99-GT-102.

[12] Casciaro, C., Treiber, M., Sell, M., 2000, "Unsteady Transport Mechanisms in an Axial Turbine", ASME Journal of Turbomachinery, Vol. 122, pp. 604-612.

[13] Favaretto, C.F.F., 2000, "Analysis of the Dynamic and Kinematic Effects on a Turbine Flowmeter", MSc Thesis (in Portuguese), Federal University of Rio Grande do Sul (UFRGS), Porto Alegre, Brazil.

[14] CFX-TASCflow Theory Documentation, 2000, AEA Technology Engineering Software Ltd., Version 2.10, Waterloo, Ontario, Canada.

[15] Brandt, A., McCormick, S.F., Ruge, J., 1984, "Sparsity and its Applications", In Evans, D.J., editor, "Algebraic Multigrid for Sparse Matrix Equations", Cambridge University Press, U.K..

[16] Hutchinson, B.R., Raithby, G.D., 1986, "A Multigrid Method based on the Additive Correction Strategy", Numerical Heat Transfer, Vol. 9, pp. 511-537.

[17] Amano, R.S., Lin, B., Song, B., 1997, "Viscous Analysis of Steam Turbine Rotor Blade Aerodynamics", ASME Paper 97-AA-7.

[18] Hildebrandt, T., Fottner L., 1999, "A Numerical Study of the Influence of the Grid Refinement and Turbulence Modeling on the Flow Field Inside a Highly Loaded Turbine Cascade", ASME Journal of Turbomachinery, Vol. 121, pp. 709-716.

[19] Kato, M., Launder, B.E., 1993, "The Modeling of Turbulent Flow Around Stationary and Vibrating Square Cylinders", 9th Symposium on "Turbulent Shear Flows".

[20] Speziale, C.G., Sarkar, S., Gatski, T.B., 1991, "Modeling the Pressure-strain correlation of turbulence: an invariant dynamical systems approach", Journal of Fluid Mechanics, 227:245-272.

[21] Tanuma, T., Shibukawa, N., Yamamoto, S., 1997, "Navier-Stokes Analysis of Unsteady Transonic Flows Through Gas Turbine Cascades with and without Coolant Ejection", ASME Paper 97-GT-479.

[22] JSME Data Book: Flow Measurements, July 1985, JSME.